energy&fuels

pubs.acs.org/EF

Article

Thermal Management of Adsorption-Based Biogas Upgrading Systems via Incorporation of Phase-Change Materials

Published as part of Energy & Fuels special issue "Celebrating Women in Energy Research".

Kyle Newport, Khaled Baamran, Ali A. Rownaghi, and Fateme Rezaei*

Cite This: *Energy Fuels* 2024, 38, 22916−22925

Read Online

ACCESS | Metrics & More | Article Recommendations | Supporting Information

ABSTRACT: Thermal management of adsorption columns is necessary to maintain their effectiveness while reducing the energy requirements of the overall separation process. In this work, we aimed at investigating the suitability of blending adsorbents with phase-change materials (PCMs) to adjust the thermal profile of a biogas upgrading column. A commercially available PCM (Nextek 28D) in quantities of 10, 20, and 30 wt % was blended with zeolite 13X in two configurations, namely, traditional pellets and 3D-printed monoliths. The use of different structures allows for better analysis of thermal profiles and assessment of the effectiveness of the PCM in a packed bed adsorption column. Due to low thermal stability, PCM was not mixed directly into the pellets and monoliths; rather, it was incorporated into the adsorption column in the form of mixed-pellet and stacked-monolith structures. Our results indicated that pelletized and stacked-monolith configurations gave rise to different degrees of heat transfer across the column. The pure 13X bed exhibited a maximum temperature of 35.8 °C at a CO_2 capacity of 2.44 mmol/g_{13X}. In comparison, while the implementation of 20 wt % PCM resulted in only an average temperature drop of 0.35 °C, the CO_2 adsorption capacity was enhanced by 11.8% per gram of 13X for mixed-pellet bed. On the other hand, the stacked-monolith bed required a minimum 20 wt % PCM to become favorable with an average temperature drop of 4.9 °C for an 8.5% increase in CO_2 uptake, but under identical conditions, the mixed-pellet bed was found to outperform the stacked-monolith counterpart. Additionally, simulation results confirmed that the energy balance shift caused by 185 J/g of PCM can be effective to lower the temperature of the column during the adsorption step, thereby improving the separation efficiency. This work highlights the potential of incorporating phase change materials into adsorption column to regulate temperature during adsorption step and increase equilibrium capacity by maintaining favorable thermodynamic conditions.

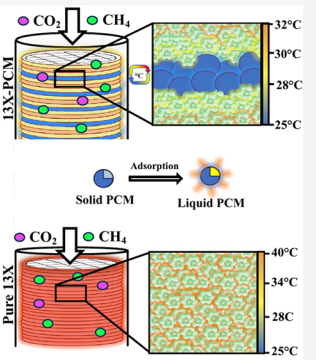

1. INTRODUCTION

In the transition toward a clean energy future, renewable fuels are gaining significant attention as more countries impose stricter policies and taxes on greenhouse gases like carbon dioxide and methane.[1] Biogas, an abundant feedstock, can serve as an alternative fuel to reduce the reliance on traditional fossil fuels for various industries.[2−4] Raw biogas coming from anaerobic digesters usually contains a large amount of CO_2 (30−40%) and a small amount of H_2S.[2,5,6] To be considered as a renewable natural gas (RNG), biogas requires approximately >97% CH_4 purity, which entails the removal of CO_2 and H_2S prior to injection into natural gas pipelines.[2,7]

While adsorption-based processes have shown promise in biogas upgrading, they remain energy-intensive and require further advancements to become economically viable on an industrial scale.[8,9] In particular, the thermal management of adsorption systems is usually problematic, as they produce large amounts of heat during adsorption due to the exothermic nature of the process, which can result in longer cooling times or lower equilibrium capacities.[10,11] Due to their high capacity, selectivity, and relatively low manufacturing cost, zeolites are the most common adsorbents for biogas upgrading.[6,12−14] However, their inherent low thermal conductivity makes the dissipation of adsorption heat throughout the column very challenging.[15,16] Coupling this with the high heat of adsorption released from the capture of CO_2 at 38−49 kJ/mol leads to long cycles or reduced pseudo-equilibrium capacity.[9,17,18] Once the heat is dissipated, the column can continue to adsorb more gas; however, this increases the cycle time and lowers the efficiency of the column.

In a recent study by Li and Li,[19] a phase-change material (PCM) with a latent heat capacity of 153 J/g was used as heat exchanger to control the thermal effects during adsorption and desorption of natural gas, and it was shown that the integration of the PCM into an adsorption tank is effective in reducing the adverse effects of adsorption heat. Later, Sakanaka et al.[20]

Received: June 25, 2024
Revised: October 25, 2024
Accepted: October 28, 2024
Published: November 17, 2024

https://doi.org/10.1021/acs.energyfuels.4c03080
Energy Fuels 2024, 38, 22916−22925

showed that integration of PCM into an adsorption column can shift the adsorbent's pseudo-equilibrium by consuming the energy to generate a phase change from solid to liquid, which, in turn, reduces the amount of heat in the column significantly, thereby increasing the adsorption capacity not only per the amount of adsorbent but also per the volume of the column. PCMs come in many forms, such as paraffin waxes and fatty acids, owing to their ability to have low-temperature phase change to dissipate surrounding heat.[11,21] In recent years, microencapsulation or copper tubes have been pursued to incorporate the PCMs.[19] Due to the high flexibility of paraffin, PCMs can be developed for many applications through adjusting the paraffin ratios. For instance, these materials have shown promise in storing latent thermal heat, allowing 5−14 times more heat storage than water.[11,21]

In this investigation, we aimed at further assessing how integration of various amounts of PCM into an adsorption column can improve the thermal management of the biogas upgrading process. Specifically, Nextek 28D was used as a PCM and blended with zeolite 13X at weight percentages of 0, 10, 20, and 30 wt % in the forms of pellets and stacked monolithic structures. Our working hypothesis was that, with identical PCM content, the heat dissipation can be drastically different for an adsorption column filled with uniformly mixed PCM/13X pellets than with stacked monoliths of PCM and 13X. Figure 1 illustrates the concept of the phase change occurrence during adsorption for a 13X/PCM bed. The dynamic breakthrough experiments were conducted with a 50/50 vol % CO_2/CH_4 feed to collect both concentration and temperature profiles, which were later used to estimate both mass and heat transfer properties of the two beds. Moreover, the viability was analyzed in comparison to filling the bed with 13X and comparing the breakthrough widths and pseudo-equilibrium capacities of the CO_2 and CH_4 gases.

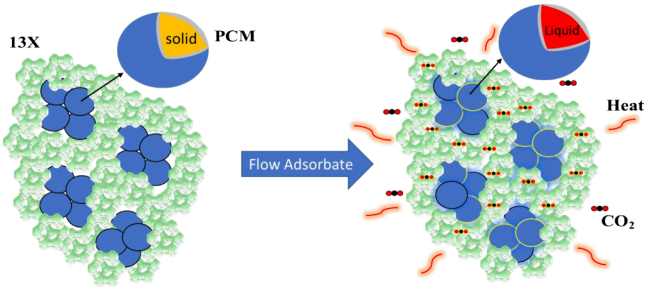

Figure 1. Schematic illustration of the phase change occurrence during adsorption for a 13X/PCM bed.

2. EXPERIMENTAL SECTION

2.1. Materials. The adsorbent zeolite 13X was obtained in a powder from Alfa Aesar with a particle size of 20 nm. Nanoparticle bentonite clay obtained from Sigma-Aldrich was used as a binder, while a shear-thinning agent, called methylcellulose, was used to help print the monoliths and later burned off during calcination to help facilitate mesoporous highways formation. The PCM called Nextek 28D was received from Microtek Laboratories in a micro-encapsulated form with a particle size of 15−30 μm and an expected heat of fusion of 185 J/g with a phase change temperature at approximately 28 °C according to Microtek. The ultra-high-purity (UHP) nitrogen and the 50/50 vol % CO_2/CH_4 cylinders were obtained from Airgas.

2.2. Monolith Printing and Pellet Extrusion. To prepare a paste, zeolite 13X was first mixed with bentonite clay and methylcellulose at a weight ratio of 87:3:10 in 10 g batches. Next, water was added to the powder, and the mixture was rolled for 48 h to ensure a homogeneous mixture. The extrudates (pellets) were extruded through a 2 mm nozzle into long strings and then cut into pieces approximately 4 mm long. The extrudates were left to dry at room temperature and then calcined at 550 °C for 6 h. Similarly, the monoliths were extruded with a 200 cell per square inch (cpsi) structure, using a 1.2 mm nozzle using a Prusa I3 A Pro three-dimensional (3D) printer, then left to dry, and calcined at 550 °C for 6 h.[13] The PCM pellets and monoliths used the same weight ratio of 87:3:10 in 10 g batches and were extruded using the same nozzle types and a heat gun to keep the material from collapsing. The PCMs were not calcined due to their low thermal stability.

2.3. Material Characterization. The textural properties of the materials were analyzed through N_2 physisorption measurements over a 3Flex gas analyzer from Micromeritics at 77 K. The non-local density functional theory (NLDFT) method was used along with the slit model to calculate the pore size distribution (PSD) profiles, while the surface areas were estimated by the Brunauer−Emmett−Teller (BET) method. Prior to the measurements, the samples were degassed at 350 °C for 6 h at a ramp rate of 10 °C/min. The same 3Flex method was used for the unary adsorption isotherms of CO_2 and CH_4, conducted at 25, 35, and 50 °C. The Clausius−Clapeyron method was then used to calculate the isosteric heat of adsorption (Q_{st}) for each gas. Additionally, the ideal-adsorbed solution theory (IAST) model was used to estimate the ideal selectivity from these isotherms. Thermogravimetric analysis (TGA Q500) was used to assess the temperature stability of 13X and PCM. The program ran from room temperature up to 900 °C at a heating rate of 10 °C/min

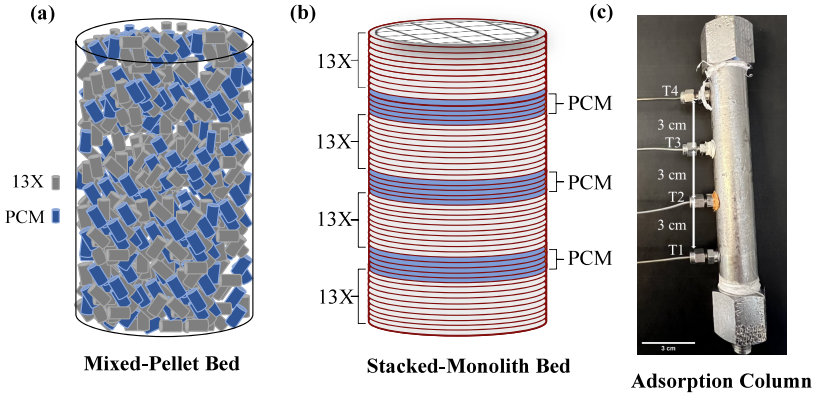

Figure 2. Schematic illustration of (a) mixed-pellet and (b) stacked-monolith beds and (c) picture of an adsorption column with four thermocouples embedded along its axial direction.

https://doi.org/10.1021/acs.energyfuels.4c03080
Energy Fuels 2024, 38, 22916−22925

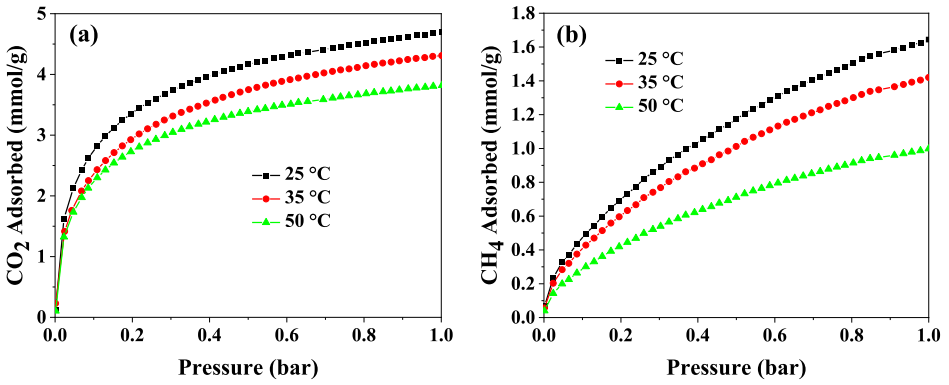

Figure 3. Unary adsorption isotherms of (a) CO_2 and (b) CH_4 at 25, 35, and 50 °C over 13X.

under N_2 gas to determine the change in the weight of the materials as a function of temperature.

2.4. Breakthrough Experiments. Two beds of adsorbents were prepared for breakthrough tests, namely, a mixed-pellet bed that contained pelletized zeolite 13X and PCM randomly loaded into the bed at weight ratios specified before (Figure 2a) and a stacked-monolith bed where monoliths of 13X and PCM, printed separately, were stacked alternatively on top of each other (Figure 2b). The total weight of the pelletized bed was 13.2 g, whereas the monolithic bed weighted 7.4 g. The pelletized 13X and PCM were mixed in a vacuum before being transferred into the column, with an intern N_2 gas flow, whereas the monolithic 13X and PCM were degassed at 100 °C over 6 h and then stacked to obtain an even distribution of PCM throughout the column. An inert flow stream of N_2 gas was used to blank the system, and then a 50:50 vol % CO_2/CH_4 feed was introduced to the 13 cm-long column with an inner diameter of 1.5 cm, as shown in Figure 2c, with four thermocouples spaced at 3 cm distances, referred to as T1, T2, T3, and T4. The maximum overall temperature change (ΔT) and average temperature change of the column (ΔT_{avg}) were reported to compare mixing inconsistencies of the PCM throughout the column. Each stream used a Brooks N_2-calibrated mass flow controller (MFC) to control the gas flow at a 100 mL/min flow rate. The outlet was analyzed using a mass flow meter (MFM) and a BelMass mass spectrometer. The material was degassed in a vacuum oven at 100 °C for 6 h.

2.5. Simulation Section. COMSOL Multiphysics 5.5 software was used to simulate concentration and temperature profiles of the pelletized and monolithic columns, based on eqs S1−S14 of the Supporting Information. These mass and energy balance equations were adopted from Sakanaka et al.[20] in our simulations. The corresponding boundary conditions and parameters are also provided in Table S3 of the Supporting Information. The partial differential equations (PDEs) obtained from mass and energy balances were solved by meshing the adsorption column with 600 tetrahedral units.

3. RESULTS AND DISCUSSION

3.1. Material Characterization. N_2 physisorption isotherms were obtained over the PCM and 13X pellets before and after adsorption experiments. The physisorption isotherms of 13X in Figure S1 of the Supporting Information display type I−IV isotherm, indicating a hierarchal microporous− mesoporous pore structure according to the International Union of Pure and Applied Chemistry (IUPAC) classification.[22−24] The shape of type H3 hysteresis loop remained consistent across fresh and spent samples, with the onset of the loop taking place at P/P_0 =0.8.[22] Zeolite 13X is an extremely characterized material, with a surface area of ∼387 m^2/g, as noted in Table S1 of the Supporting Information.[25,26] The surface area of the zeolite 13X pellet/monolith was slightly lower than that reported in the literature (ca. 400−800 m^2/g) due to the addition of the bentonite clay binder.[23,24] The PCM possessed a surface area of 17 m^2/g, as expected. This low surface area was due to the lack of a porous structure from its encapsulated structure. The role of the PCM was to provide latent heat storage during adsorption; therefore, it was not necessary to possess a large surface area.

3.2. Unary CO_2 and CH_4 Adsorption Isotherms. The unary adsorption isotherms of CO_2 and CH_4 over the bare zeolite were obtained at 25, 35, and 50 °C, as shown in Figure 3. In agreement with the literature, the bare zeolite 13X was more selective toward CO_2 than CH_4, reaching capacities comparable to the reported data of 4.7 and 1.7 mmol/g, respectively, at 1 bar. It should be noted here that the PCM did not exhibit any affinities toward the two adsorbates. Therefore, one may expect that the addition of PCM cannot increase the adsorption of CO_2 or CH_4 when it is added to the column. However, this was not the case as the PCM's ability to store heat upon phase change allowed the adsorbent to continue adsorbing more molecules at a lower temperature. The adsorbent experienced 8.20 and 18.6% reduction in CO_2 uptake as temperature increased from 25 to 35 and 50 °C, respectively and 13.7 and 39.2% in the adsorption capacity of CH_4.[19−21,27] The Q_{st} values of CO_2 and CH_4 were estimated from these isotherms, as presented in Table S2 of the Supporting Information, along with the theoretical selectivity values from the IAST method for use in the COMSOL simulations. The large heat release noted from the Q_{st} values (47.9 and 21.5 kJ/mol for CO_2 and CH_4, respectively) can lead to significant capacity losses during adsorption step. Furthermore, CO_2/CH_4 selectivity value of 7.5 was estimated from the IAST model for our 13X adosrbent, which was in agreement with the literature data. It should be pointed out here that PCM and 13X were also printed directly within a composite structure; however, this incorporation method was discarded due torelatively large adsorption capacity losses, as shown in Figure S3 of the Supporting Information, which stemmed from pore blockage of 13X with a reduction of 39 and 16.3% for CO_2 and CH_4 gases, respectively. Therefore, the experimental results were conducted using separate 13X and PCM structures mixed in a column in the forms of pellets and monoliths.

3.3. Dynamic Breakthrough Experiments. *3.3.1. Effect of PCM Loading.* As noted earlier, zeolite 13X is known for its preferential adsorption of CO_2 over CH_4, which can in turn increase the bed temperature significantly due to much higher Q_{st} of CO_2 than that of CH_4. Thus, finding ways to shift the adsorption equilibrium by lowering the bed temperature

https://doi.org/10.1021/acs.energyfuels.4c03080
Energy Fuels 2024, 38, 22916−22925

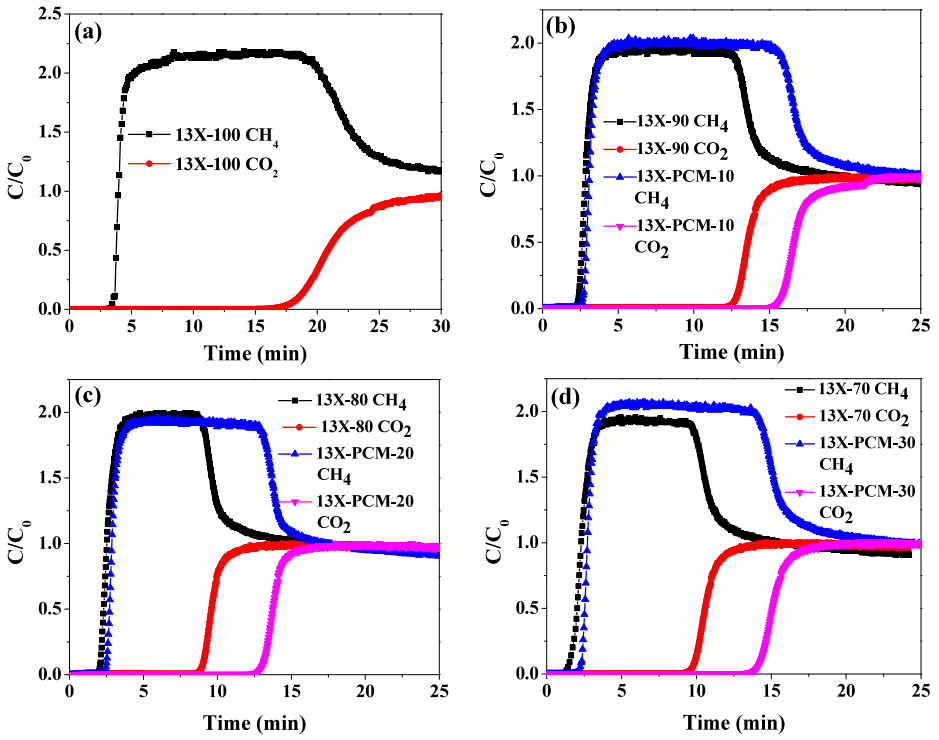

Figure 4. Concentration profiles for (a) 13X-100 and mixed-pellet beds with (b) 13X−PCM-10, (c) 13X−PCM-20, and (d) 13X−PCM-30.

Table 1. Breakthrough Parameters for the Mixed-Pellet Beds with (b) 13X−PCM-10, (c) 13X−PCM-20, and (d) 13X−PCM-30 at 25 °C, 1 bar, and a Flow Rate of 100 mL/min

adsorbent	t_{95CO_2} (min)	t_{95CH_4} (min)	q_{CO_2} (mmol/g)	q_{CH_4} (mmol/g)	ΔT (°C)	ΔT_{avg} (°C)
13X-100	29.4	4.10	2.44	0.48	38.5	9.63
13X-90	16.4	3.60	2.42	0.46	35.3	8.82
13X−PCM-10	21.6	3.70	3.01	0.51	37.4	9.35
13X-80	11.4	3.10	2.34	0.35	30.0	7.54
13X−PCM-20	15.2	3.30	2.73	0.50	32.8	8.20
13X-70	13.0	3.65	2.31	0.47	27.1	9.03
13X−PCM-30	16.0	3.70	2.65	0.56	31.2	7.84

during adsorption can be advantageous in biogas upgrading process over zeolite 13X. Here, we aimed at assessing how PCM with varied loading can enable the shift in adsorption equilibrium when mixed with 13X in mixed-pellet and stacked-monolith configurations. Additionally, we tested fully loaded (bare)13X beds with the same weight as benchmarks for comparison to the three PCM−13X beds. The concentration profiles for the pure 13X column (13X-100) are provided in Figure 4a, which show a much wider breakthrough width (7.8 min vs. 1.2 min) and a longer breakthrough time for CO_2 than for CH_4 (17.8 min vs. 3.4 min).[28] The concentration profiles of the mixed-pellet beds in panels b−d of Figure 4 show longer breakthrough times for both CO_2 and CH_4 relative to those for the corresponding bare13X beds. The breakthrough parameters are given in Table 1. As noted from these data, the incorporation of the PCM enhanced the pseudo-equilibrium capacity of CO_2 (q_{CO_2}) by 19.6, 14.2, and 12.8% for 13X-PCM-10, 13X-PCM-20, and 13X-PCM-30 columns, respectively. Similarly, the corresponding temperature profiles in Figure 5 indicate that the average temperature of the column increased in 10, 20, 30 wt % 13X−PCM by 5.67, 13.3, and 4.24%, respectively, upon incorporation of the PCM. The only source of heat in the system at this stage was Q_{st} of CO_2 and CH_4 gases; therefore, the additional energy input into the system contributed to higher adsorption of both gases. Due to the additional gas uptake, there was an expected temperature increase of 3.7 °C for the 13X-PCM-10, 3.2 °C for the 13X-PCM-20, and 2.9 °C for 13X-PCM-30, as estimated from the heats of adsorption as well as the heat capacity of 13X. Nevertheless, the overall temperature of the column was reduced by 1.8, 2.8, and 4.2 °C for 13X-PCM-10, 13X-PCM-20, and 13X-PCM-30, respectively, when not accounting for any additional gas uptake by 13X. Non-uniform mixing and clumping of the PCM can account for the reduced performance of the 20 and 30 wt % PCM columns; therefore, more stable PCMs would further increase the effectiveness of the system through increased incorporation into the structured adsorbents. Moreover, the addition of 10 wt % PCM (13X-PCM-10) gave rise to the ΔT_{avg} of 9.35 °C, whereas 13X-PCM-20 and 13X-PCM-30 beds displayed ΔT_{avg} of 8.20 and 7.84 °C, respectively. On the basis of these results, we concluded that the PCM loading in the range of 10−30 wt % provides a suitable balance between the increased adsorption capacity of 13X and a reduced average temperature of the column during adsorption step.[20]

https://doi.org/10.1021/acs.energyfuels.4c03080
Energy Fuels 2024, 38, 22916−22925

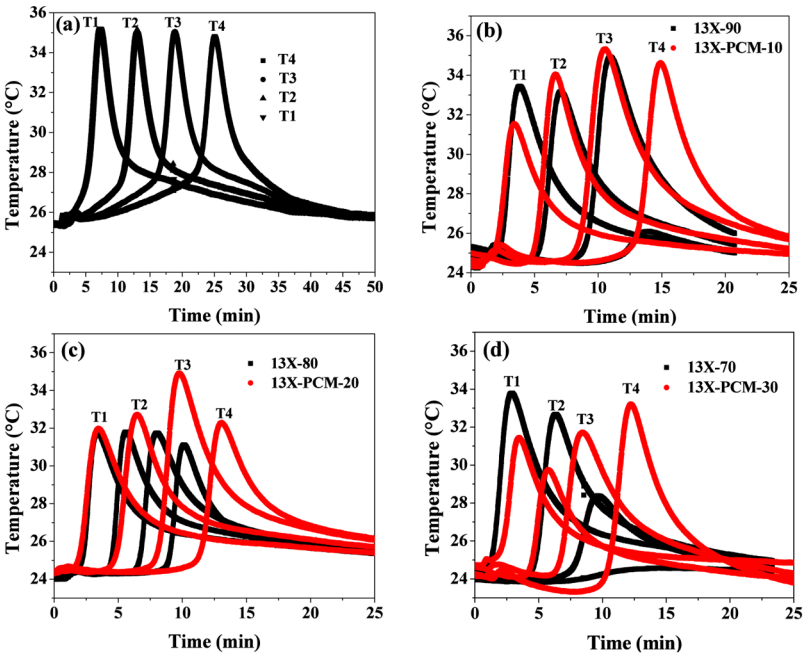

Figure 5. Temperature profiles for (a) 13X-100 and mixed-pellet beds with (b) 13X−PCM-10, (c) 13X−PCM-20, and (d) 13X−PCM-30.

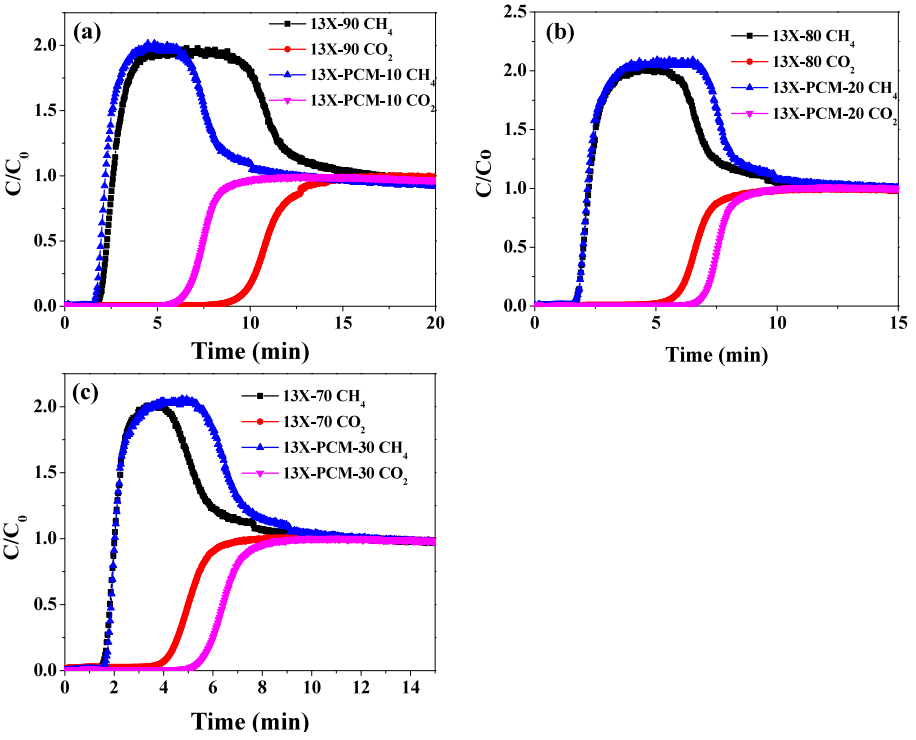

Figure 6. Concentration profiles for the stacked-monolith beds with (a) 13X−PCM-10, (b) 13X−PCM-20, and (c) 13X−PCM-30.

In comparison to the 13X-100 column, the CO_2 breakthrough time reduced by ∼12% in the 13X-PCM-10. However, when the gas uptake was compared per 13X weight, the CO_2 and CH_4 capacities were increased by 18.9 and 6.25%, respectively. The increased gas uptake further indicated that the PCM caused an effective increase per gram of adsorbent; however, the increased adsorption did not overcome the additional adsorption from the increased quantity of 13X in the column. The PCM presence in the column led to a significant decrease in the average column temperature over the bare 13X column of 0.275, 0.930, and 0.438 °C for the 10, 20, and 30 wt % 13X−PCM columns, respectively. The PCM is hypothesized to prolong the adsorption step by absorbing exothermic heat through its latent heat capacity. By moderating temperature increases during adsorption, the PCM can help maintain favorable conditions for adsorption and potentially allow for faster cycle times. This was the case here as cycle times of 7.80, 14.2, and 13.4 min were noted for 10, 20, and 30 wt % 13X−PCM columns, respectively (if cycled at 95% adsorption of CO_2). Nonetheless, it is important to balance the PCM and

https://doi.org/10.1021/acs.energyfuels.4c03080
Energy Fuels 2024, 38, 22916−22925

Table 2. Breakthrough Parameters for the Stacked-Monolith Beds with (a) 13X−PCM-10, (b) 13X−PCM-20, and (c) 13X−PCM-30 at 25 °C, 1 bar, and a Flow Rate of 100 mL/min

adsorbent	$t_{95adsCO_2}$ (min)	t_{95CH_4} (min)	q_{CO_2} (mmol/g)	q_{CH_4} (mmol/g)	ΔT (°C)	ΔT_{avg} (°C)
13X-90	11.4	1.98	2.46	0.70	37.2	9.30
13X−PCM-10	7.21	1.90	2.34	0.68	37.1	9.27
13X-80	6.27	1.98	2.36	0.70	20.9	6.97
13X−PCM-20	7.58	1.97	2.68	0.69	16.0	4.28
13X-70	6.58	1.18	2.20	0.45	10.9	3.63
13X−PCM-30	8.00	2.04	2.61	0.74	10.2	2.92

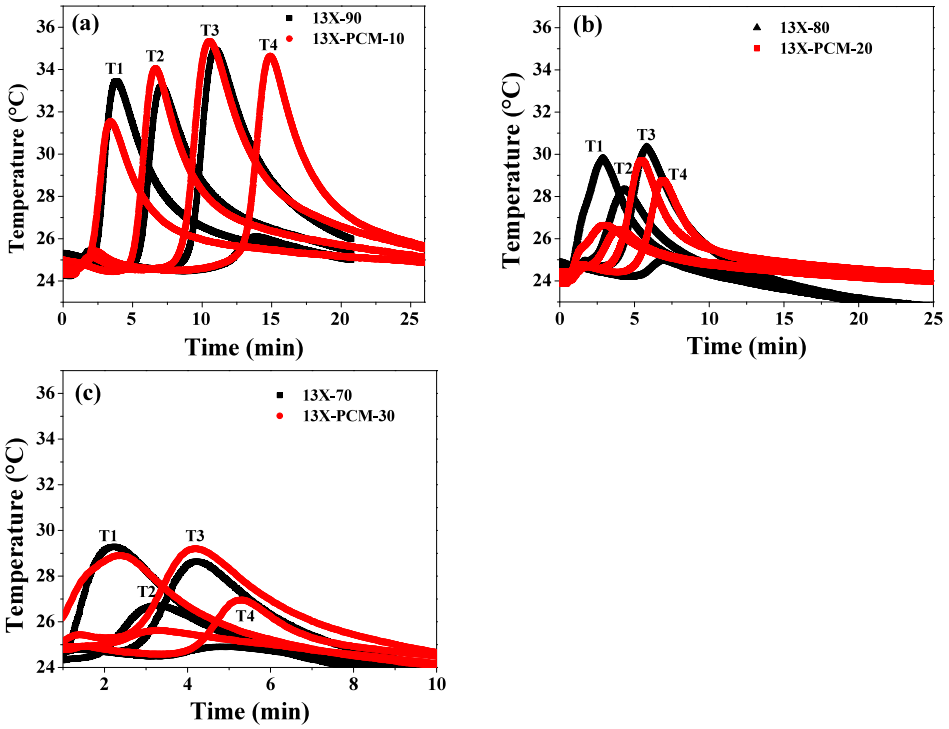

Figure 7. Temperature profiles for the stacked-monolith beds with (a) 13X−PCM-10, (b) 13X−PCM-20, and (c) 13X−PCM-30.

adsorbent loadings as the PCM can only affect the surrounding particles and will, therefore, become less effective at lower adsorption percentages.

3.3.2. Effect of Bed Structure. After demonstrating that a relatively low PCM content is effective in promoting the performance of 13X in biogas upgrading, the 13X/PCM bed configuration was switched from pellet to monolith to investigate the effectiveness of PCM in the context of structured bed. The monolithic 13X was stacked on thin layers of PCM to evenly distribute the PCM throughout the column with 2 cm tall 13X monoliths stacked on 5 mm PCM monoliths. Monolithic structures are known to decrease the pressure drop by 60%, which is beneficial for large scale operations.[29] As shown in Figure 6, the PCM at the 10 wt % loading reduced the 13X CO_2 uptake by 4.87%, which could be associated with the limited contact between the 13X and PCM monoliths. As the PCM loading was increased from 10 to 20 and 30 wt %, it was more evenly distributed throughout the column and utilized more heat through the phase change, causing an increase in the pseudo-equilibrium capacity of CO_2 by 11.9 and 15.7%, respectively. This can also be inferred from the estimated ΔT data in Table 2, highlighting that in the case of 13X-PCM−10, the amount of PCM was not sufficient to spread throughout the column and hence make a noticable impact, as it reduced the average column temperature by only 0.32%. However, as the concentration of PCM increased throughout the column, the heat was reduced for 13X-PCM-20 and 13X-PCM-30 samples by 38.6 and 19.5%, respectively, relative to their corresponding bare 13X-80 and 13X-70 counterparts. This heat reduction can also be observed from the temperature profiles of the column in Figure 7, which closely resembled those for the corresponding bare 13X for the 13X-PCM-10 sample (in Figure 7a), while Figure 7 b-c start to see a reduction in the overall temperature profiles for 13X-PCM-20 and 13X-PCM-30 samples. The trend also indicated that the materials were cooling faster than their bare 13X counterparts.

Overall, comparison of the results of the pelletized and monolithic beds indicated that the pelletized structure was more effective than its stacked analogue in reducing the bed temperature during adsorption step and increasing the breakthrough time of both CO_2 and CH_4. This could be attributed to a more uniform distribution of PCM pellets throughout the column, allowing heat to dissipate more easily as opposed to the PCM distribution in the monolithic bed, which was more concentrated in layers with less contact with the 13X particles. Therefore, not all the PCM was utilized due to the higher localization, which caused larger fluctuations

https://doi.org/10.1021/acs.energyfuels.4c03080
Energy Fuels 2024, 38, 22916−22925

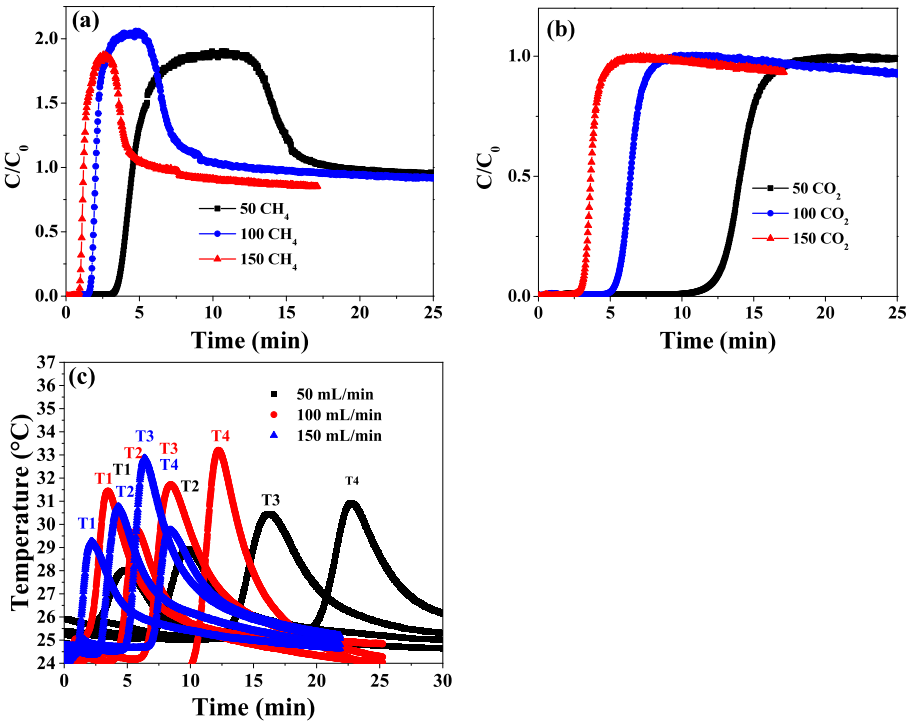

Figure 8. Concentration profiles of (a) CH_4 and (b) CO_2 and (c) corresponding temperature profiles along the PCM−13X-30 stacked-monolith bed at 50, 100, and 150 mL/min flow rates.

throughout the column, as evident in Figure 7. The breakthrough time decrease of the monoliths was caused by the decreased adsorbent packing weight of 44.0%, causing a reduction in the monolithic CO_2 breakthrough time by 50.1%. The reduction in the adsorption packing resulted from column limitations caused by the addition of thermocouples into the system. However, this can be increased through column optimization and applying higher cell-density monoliths. An alternative to the stacked configuration would be to fully incorporate PCM into the monolith by premixing it with the adsorbent; however, this method was deemed unsuccessful.

3.3.3. Effect of Feed Flow Rate. It is important to evaluate the temperature fluctuations during adsorption at different feed flow rates to better assess the role of PCM in managing thermal effects at a wide range of operationing conditions. The flow rates were varied from 50 to 100 and 150 mL/min for the 13X−PCM-30 stacked-monolith column. Although the range studied here is much smaller than that used in conventional pilot plants of 1.5−2.5 m^3/h, it is still wide enough for a valid analysis at the lab scale.[14,30] As expected, the column experienced higher temperature spikes at higher flow rates (Figure 8c), mainly due to faster kinetics and shorter time for heat dissipation.[31] Specifically, ΔT_{avg} values were estimated to be 4.25, 6.32, and 7.88 °C for 50, 100, and 150 mL/min flow rates, respectively. It should be noted here that the intrinsic heats of adsorption of CO_2 and CH_4 are essentially independent of feed flow rate and remain constant over the course of adsorption. Examinaton of the data in Table 3 revealed that the PCM was more effective at higher feed flow rates in dissipating the rapid buildup of heat generated upon adsorption, giving rise to a bed temperature of ∼33.8 °C at 150 mL/min. Moreover, the CO_2 breakthrough time reduced by 51.7 and 69.4% for 100 and 150 mL/min flow rates, respectively, compared to the 50 mL/min flow rate (Figure 8b), which translated into capacity losses of 6.78 and 20.7%.

Table 3. Breakthrough Parameters for the 13X−PCM-30 Stacked-Monolith Bed at 50, 100, and 150 mL/min

feed flow rate (mL/min)	$t_{95adsCO_2}$ (min)	t_{95CH_4} (min)	q_{CO_2} (mmol/g)	q_{CH_4} (mmol/g)	ΔT_{avg} (°C)
50	16.6	4.82	2.80	0.79	4.25
100	8.01	2.43	2.61	0.74	6.32
150	5.08	1.64	2.22	0.63	7.88

Overall, this analysis indicated that the role of PCM in managing the thermal effects can be more pronounced at higher feed flow rates where reduced heat dissipation can cause localized heat buildup around adsorption sites. This of course requires utilization of a more thermally-stable PCM that undergoes phase change at high temperatures to effectively lower the bed temperature.

3.4. PCM Limitations. PCMs are usually selected based on a specific target temperature range that they can control. In this case, the Nextech 28D was chosen for proximity of its phase change temperature (28 °C) to room temperature and its cost effectiveness. Additionally, this paraffin-based PCM was utilized to enable the fabrication of monolithic structures without a change in chemical composition. Other low-temperature PCMs, such as salt hydrates, are not viable for the present application due to solvent−salt interactions in the printing process.[32−34] To better investigate the effect of the PCM on the adsorption performance of 13X in the biogas upgrading process, we analyzed the spent 13X pellets (from a mixed-pellet bed) after adsorption (and desorption) test via TGA and N_2 physisorption measurements, and compared the results to those of fresh 13X pellets. Weighing the 13X pellets after the experiment also indicated weight gain, suggesting that some PCM might have been stuck in the pores of the 13X pellets. The TGA profiles in Figure S2 of the Supporting Information further verified that the PCM was melting out of

https://doi.org/10.1021/acs.energyfuels.4c03080
Energy Fuels 2024, 38, 22916−22925

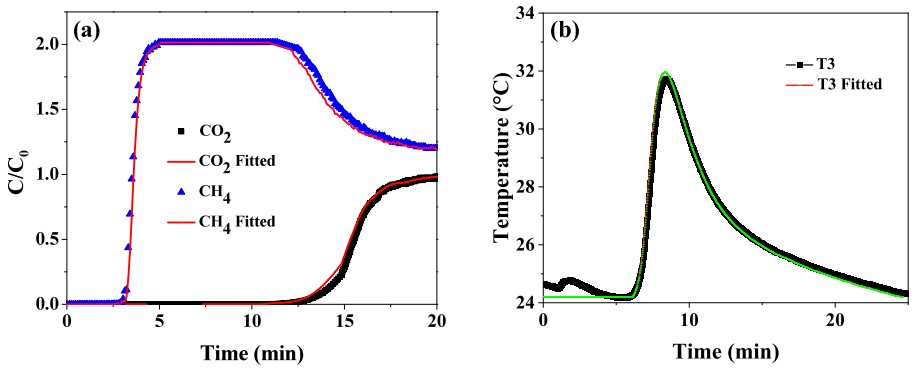

Figure 9. Fitted and experimental concentration profiles of (a) CO_2 and CH_4 and (b) corresponding temperature profile for the 13X−PCM-30 mixed-pellet bed.

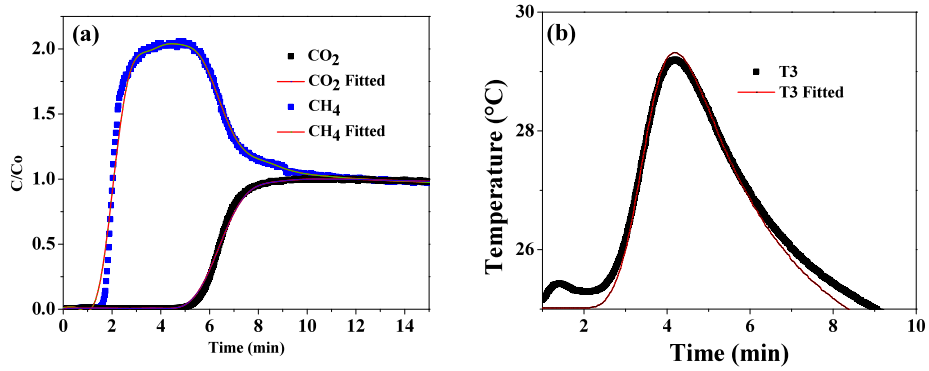

Figure 10. Fitted and experimental concentration profiles of (a) CO_2 and CH_4 and (b) corresponding temperature profile for the 13X−PCM-30 stacked-monolith bed.

the capsule and leaking into the pores of the 13X pellets between 100 and 150 °C, which normally only releases water within this temperature range. The weight losses for fresh and spent samples up to 350 °C were calculated to be 73 and 78%, respectively. Moreover, the N_2 physisorption isotherms in Figure S1 of the Supporting Information indicated that N_2 uptake over the spent sample was reduced dramatically due to pore blockage caused by migration of the PCM into the pores during the phase change process. If decomposed, PCM tends to leak into the pores of adsorbent, causing a decrease in the surface area and pore volume. As noted in Table S1 of the Supporting Information, after regeneration, the surface area (S_{BET}) and mesopore volume (V_{meso}) reduced by ∼19 and 52%, respectively, while the micropore volume (V_{micro}) diminished completely. This issue can be addressed by properly encapsulating the PCM into materials other than paraffin. Indeed, temperature-stable encapsulation of PCMs has become popular for use in high-temperature applications, but it is still in development. For instance, Zhao et al. developed micro-encapsulated PCMs containing paraffin by chemical precipitation and complexation using SiO_2 and HKUST-1 and demonstrated their performance as shape-stabilized thermal energy storage materials.[33,35] In conclusion, for an effective PCM-incorporated adsorption column to work closely with adsorbent particles, a suitable nanoencapsulation method should be utilized in the synthesis of the PCMs.

3.5. Simulated Profiles. The simulated COMSOL concentration profiles of CO_2 and CH_4 and the respective temperature profile (T3) for the PCM−13X-30 mixed-pellet and stacked-monolith beds are presented in Figures 9 and 10, respectively, and the corresponding calculated parameters are listed in Table 4, where $k_{CO_2,overall}$ and $k_{CH_4,overall}$ are the mass transfer coefficients for CO_2 and CH_4, respectively, h_{BW} is the heat transfer coefficient between the packed bed and the column wall, and U_{BPW} is the overall heat transfer coefficient between the adsorbent and the PCM. The simulated profiles of the 13X-100 column are also presented in Figure S4 of the Supporting Information. Examination of the concentration profiles obtained from simulation and experiments yielded a R^2 of 96.2%. It should be noted here that the temperature profiles were simulated by assuming that the PCM was uniformly distributed throughout the column; however, this was not the case in our experiments due to the non-uniform mixing of the PCM and 13X pellets. This non-uniform mixing led to a relatively large error in the simulated temperature profiles, as the experimental data exhibited fluctuations that were not observed in the simulations. Nonetheless, while the simulated data did not directly match the peak temperature values of the

Table 4. Estimated Mass and Heat Transfer Coefficients for the Three Columns

parameter	13X pellet	13X−PCM-30 pellet	13X−PCM-30 monolith
$k_{CO_2,overall}$ (s^{-1})	0.0054	0.0061	0.0047
$k_{CH_4,overall}$ (s^{-1})	0.0019	0.0022	0.0016
h_{BW} (J m^{-2} K^{-1})	89	95	91
U_{BPW} (J m^{-2} K^{-1})	48	55	50

https://doi.org/10.1021/acs.energyfuels.4c03080
Energy Fuels 2024, 38, 22916−22925

experimental data, the overall average temperature fluctuations of the column in both cases showed similar trends, indicating that the presence of the PCM lowered the overall bed temperature, thereby promoting the adsorption capacity of both CO_2 and CH_4. Furthermore, the kinetic parameters of CO_2 and CH_4 were on the same order of magnitude, indicating that the chosen parameters for simulation were a good representation of the system.[36] From the estimated parameters in Table 4, it is evident that the 13X−PCM mixed-pellet bed exhibited enhanced kinetics, as the $k_{CO_2,overall}$ and $k_{CH_4,overall}$ values increased by 12.9 and 13.6%, respectively, relative to those for the bare 13X bed. Because the PCM does not adsorb any gases to prolong the breakthrough, it was further indicated that this change was caused primarily by the thermal modification of the system, as indicated by the increase in U_{BPW} (by 11.1%). Comparing the temperature profiles of the 13X−PCM-30 mixed-pellet and stacked-monolith beds in Figures 9b and 10b to that for the 13X-100 bed in Figure S4b of the Supporting Information, a relatively significant reduction in the average bed temperature (∼7.24%) was noted, which increased breakthrough time of both CO_2 and CH_4, as indicated before.

For the 13X−PCM-30 stacked-monolith bed on the other hand, $k_{CO_2,overall}$ was estimated to be 0.0047 s^{-1}, which was 12.9 and 22.9% lower than those for 13X and 13X−PCM-30 mixed-pellet beds, respectively, with a similar decrease in the CH_4 kinetics (0.0016 vs. 0.0019 and 0.0022 s^{-1}, respectively). The smaller kinetic parameters could hint at reduced capacity, which was caused by reduced column density and increased bypass seen in monolithic samples. The U_{BPW} values showed a small increase of 4.06% over the bare 13X sample but was 9.09% lower than that of the pelletized 13X−PCM-30 column. The enhancement over the bare 13X but below the mixed-pellet columns indicated that the PCM incorporation into the monolithic bed was beneficial but not to the same extent as in the pelletized column due to the reduction in the contact area between the PCM and the 13X.

4. CONCLUSION

Thermal management of adsorptive separation systems requires a careful design of adsorbent materials and adsorption columns to effectively dissipate the heat generated during the adsorption step. In that regard, utilization of PCMs that can undergo phase change during adsorption and desorption steps can be considered as a practical way toward adsorption columns' heat management. However, issues with the thermal instability of the PCM necessiate a more thermally stable encapsulation method at higher temperatures to keep the material from hindering the pores of the adsorbent. If addressed, then the material could be mixed directly into the pellets or monoliths with adsorbent particles, allowing for an even more effective heat dissipation and a more homogeneous mixture to better dissipate the heat throughout the column. Our results showed that the mixed-pellet bed was more effective than the stacked-monolith counterpart due to the uniform mixing of the pellets in the column and a closer contact between PCM and 13X pellets. As indicated by dynamic breakthrough results, incorporation of 10 wt % PCM into the pelletized bed allowed for an increase in CO_2 uptake, however, it took a minimum of 20 wt % PCM to increase the capacity of the monolith due to uneven loading of PCM in the column. Additionally, the mixed-pellet bed led to an increase in the column temperature of up to 4.8 °C. The PCM was effective at 20 and 30 wt % in the stacked-monolith bed, while increasing the PCM concentration beyond 30 wt % lowered the adsorption temperature below the 28 °C PCM threshold, reducing the overall system's effectiveness. The capture capacity was still lower on a volumetric basis than if the column were filled with pure 13X, though.

■ ASSOCIATED CONTENT

Supporting Information

The Supporting Information is available free of charge at https://pubs.acs.org/doi/10.1021/acs.energyfuels.4c03080.

Material characterization results, COMSOL simulation parameters, material and energy balance equations, and nomenclature (PDF)

■ AUTHOR INFORMATION

Corresponding Author

Fateme Rezaei − *Department of Chemical, Environmental and Materials Engineering, University of Miami, Miami, Florida 33124, United States;* orcid.org/0000-0002-4214-4235; Email: rezaeif@miani.edu

Authors

Kyle Newport − *Department of Chemical & Biochemical Engineering, Missouri University of Science and Technology, Rolla, Missouri 65409-1230, United States*

Khaled Baamran − *National Energy Technology Laboratory (NETL), United States Department of Energy, Pittsburgh, Pennsylvania 15236, United States*

Ali A. Rownaghi − *National Energy Technology Laboratory (NETL), United States Department of Energy, Pittsburgh, Pennsylvania 15236, United States;* orcid.org/0000-0001-5228-5624

Complete contact information is available at: https://pubs.acs.org/10.1021/acs.energyfuels.4c03080

Notes

The authors declare no competing financial interest.

■ ACKNOWLEDGMENTS

The authors thank the National Science Foundation for financially supporting this project through Grant NSF-PFI-2044726.

■ REFERENCES

(1) Creutzig, F. Fuel Crisis Slash Demand in Three Sectors. *Nature* **2022**, *606*, 460−462.

(2) Weiland, P. Biogas Production: Current State and Perspectives. *Appl. Microbiol. Biotechnol.* **2010**, *85*, 849−860.

(3) Speight, J. G. *Natural Gas: A Basic Handbook*; Gulf Professional Publishing: Houston, TX, 2018; DOI: 10.1002/9781119240297.

(4) Al-Mamoori, A.; Krishnamurthy, A.; Rownaghi, A. A.; Rezaei, F. Carbon capture and utilization update. *Energy Technol.* **2017**, *5*, 834−849.

(5) Bauer, F.; Persson, T.; Hulteberg, C.; Tamm, D. Biogas Upgrading—Technology Overview, Comparison and Perspectives for the Future. *Biofuels, Bioprod. Biorefin.* **2013**, *7* (5), 499−511.

(6) Al-Naddaf, Q.; Lawson, S.; Rownaghi, A. A.; Rezaei, F. Analysis of Dynamic CO_2 Capture over 13X Zeolite Monoliths in the Presence of SO_x, NO_x and Humidity. *AIChE J.* **2020**, *66* (9), e16297.

(7) European Commission (EC). *Energy Roadmap 2050*; EC: Brussels, Belgium, 2012; DOI: 10.2833/10759.

(8) Aromada, S. A.; Eldrup, N. H.; Normann, F.; Øi, L. E. Techno-Economic Assessment of Different Heat Exchangers for CO_2 Capture. *Energies* **2020**, *13* (23), 6315.
(9) Prado, D. S.; Vilarrasa-García, E.; Sampronha, E.; Beleli, Y. S.; Moreira, F. S.; Paiva, J. L.; Roux, G. A. C. L.; Bastos-Neto, M.; Azevedo, D. C. S.; Silva, E. C. N.; Seckler, M. M. Multiple Approaches for Large-Scale CO_2 Capture by Adsorption with 13X Zeolite in Multi-Stage Fluidized Beds Assessment. *Adsorption* **2024**, *30* (5), 429−455.
(10) Elfving, J.; Bajamundi, C.; Kauppinen, J.; Sainio, T. Modelling of Equilibrium Working Capacity of PSA, TSA and TVSA Processes for CO_2 Adsorption under Direct Air Capture Conditions. *J. CO_2 Util.* **2017**, *22*, 270−277.
(11) Wu, S.; Yan, T.; Kuai, Z.; Pan, W. Thermal Conductivity Enhancement on Phase Change Materials for Thermal Energy Storage: A Review. *Energy Storage Mater.* **2020**, *25*, 251−295.
(12) Lu, C.; Bai, H.; Wu, B.; Su, F.; Hwang, J. F. Comparative Study of CO_2 Capture by Carbon Nanotubes, Activated Carbons, and Zeolites. *Energy Fuels* **2008**, *22*, 3050−3056.
(13) Lawson, S.; Adebayo, B.; Robinson, C.; Al-Naddaf, Q.; Rownaghi, A. A.; Rezaei, F. The Effects of Cell Density and Intrinsic Porosity on Structural Properties and Adsorption Kinetics in 3D-Printed Zeolite Monoliths. *Chem. Eng. Sci.* **2020**, *218*, 115564.
(14) Henrotin, A.; Heymans, N.; Duprez, M. E.; Mouchaham, G.; Serre, C.; Wong, D.; Robinson, R.; Mulrooney, D.; Casaban, J.; De Weireld, G. Lab-Scale Pilot for CO_2 Capture Vacuum Pressure Swing Adsorption: MIL-160(Al) vs Zeolite 13X. *Carbon Capture Sci. Technol.* **2024**, *12*, 100224.
(15) Aittomäki, A.; Aula, A. Determination of Effective Thermal Conductivity of Adsorbent Bed Using Measured Temperature Profiles. *Int. Commun. Heat Mass Transfer* **1991**, *18* (5), 681−690.
(16) Jaya, N. A.; Yun-Ming, L.; Cheng-Yong, H.; Abdullah, M. M. A. B.; Hussin, K. Correlation between Pore Structure, Compressive Strength and Thermal Conductivity of Porous Metakaolin Geopolymer. *Constr. Build. Mater.* **2020**, *247*, 118641.
(17) Son, K. N.; Cmarik, G. E.; Knox, J. C.; Weibel, J. A.; Garimella, S. v. Measurement and Prediction of the Heat of Adsorption and Equilibrium Concentration of CO_2 on Zeolite 13X. *J. Chem. Eng. Data* **2018**, *63* (5), 1663−1674.
(18) Giraldo, L.; Rodriguez-Estupiñán, P.; Moreno-Piraján, J. C. Isosteric Heat: Comparative Study between Clausius−Clapeyron, CSK and Adsorption Calorimetry Methods. *Processes* **2019**, *7* (4), 203.
(19) Li, X.; Li, Y. Applications of Organic Phase Change Materials Embedded in Adsorbents for Controlling Heat Produced by Charging and Discharging Natural Gas. *Adsorption* **2015**, *21* (5), 383−389.
(20) Sakanaka, Y.; Hiraide, S.; Tanaka, H.; Hiratsuka, T.; Kojima, N.; Yamane, Y.; Miyahara, M. T. Efficiency of Thermal Management Using Phase-Change Material for Nonisothermal Adsorption Process. *Ind. Eng. Chem. Res.* **2020**, *59* (32), 14485−14495.
(21) Sharma, A.; Tyagi, V. V.; Chen, C. R.; Buddhi, D. Review on Thermal Energy Storage with Phase Change Materials and Applications. *Renewable Sustainable Energy Rev.* **2009**, *13*, 318−345.
(22) Thommes, M.; Kaneko, K.; Neimark, A. V.; Olivier, J. P.; Rodriguez-Reinoso, F.; Rouquerol, J.; Sing, K. S. W. Physisorption of Gases, with Special Reference to the Evaluation of Surface Area and Pore Size Distribution (IUPAC Technical Report). *Pure Appl. Chem.* **2015**, *87* (9−10), 1051−1069.
(23) Chen, C.; Park, D. W.; Ahn, W. S. CO_2 Capture Using Zeolite 13X Prepared from Bentonite. *Appl. Surf. Sci.* **2014**, *292*, 63−67.
(24) Garshasbi, V.; Jahangiri, M.; Anbia, M. Equilibrium CO_2 Adsorption on Zeolite 13X Prepared from Natural Clays. *Appl. Surf. Sci.* **2017**, *393*, 225−233.
(25) Sowunmi, A. R.; Folayan, C. O.; Anafi, F. O.; Ajayi, O. A.; Omisanya, N. O.; Obada, D. O.; Dodoo-Arhin, D. Dataset on the Comparison of Synthesized and Commercial Zeolites for Potential Solar Adsorption Refrigerating System. *Data Brief* **2018**, *20*, 90−95.
(26) Newport, K.; Baamran, K.; Rownaghi, A. A.; Rezaei, F. Magnetic-Field Assisted Gas Desorption from Fe_2O_3/Zeolite 13X Sorbent Monoliths for Biogas Upgrading. *Ind. Eng. Chem. Res.* **2022**, *61* (51), 18843−18853.
(27) Shchukina, E. M.; Graham, M.; Zheng, Z.; Shchukin, D. G. Nanoencapsulation of Phase Change Materials for Advanced Thermal Energy Storage Systems. *Chem. Soc. Rev.* **2018**, *47*, 4156−4175.
(28) Álvarez-Gutiérrez, N.; Gil, M. V.; Rubiera, F.; Pevida, C. Kinetics of CO_2 Adsorption on Cherry Stone-Based Carbons in CO_2/CH_4 Separations. *Chem. Eng. J.* **2017**, *307*, 249−257.
(29) Lawson, S.; Li, X.; Thakkar, H.; Rownaghi, A. A.; Rezaei, F. Recent Advances in 3D Printing of Structured Materials for Adsorption and Catalysis Applications. *Chem. Rev.* **2021**, *121*, 6246−6291.
(30) Rajivgandhi, M. M. C.; Singaravelu, M. Upgrading Biogas to Biomethane by Physical Absorption Process. *Int. J. Agric., Environ. Biotechnol.* **2014**, *7* (3), 639.
(31) Mulgundmath, V. P.; Jones, R. A.; Tezel, F. H.; Thibault, J. Fixed Bed Adsorption for the Removal of Carbon Dioxide from Nitrogen: Breakthrough Behaviour and Modelling for Heat and Mass Transfer. *Sep. Purif. Technol.* **2012**, *85*, 17−27.
(32) Khan, Z.; Khan, Z.; Ghafoor, A. A Review of Performance Enhancement of PCM Based Latent Heat Storage System within the Context of Materials, Thermal Stability and Compatibility. *Energy Convers. Manage.* **2016**, *115*, 132−158.
(33) Cárdenas-Ramírez, C.; Jaramillo, F.; Gómez, M. Systematic Review of Encapsulation and Shape-Stabilization of Phase Change Materials. *J. Energy Storage* **2020**, *30*, 101495.
(34) Castell, A.; Solé, C. An Overview on Design Methodologies for Liquid−Solid PCM Storage Systems. *Renewable Sustainable Energy Rev.* **2015**, *52*, 289−307.
(35) Zhao, L.; Li, J.; Duan, X.; Wang, S. Microencapsulated Paraffin with SiO_2 and Cu-BTC Composite Shell as Shape-Stabilized Thermal Energy Storage Materials. *Energy Build.* **2023**, *290*, 113102.
(36) Zhang, Z.; Zhang, W.; Chen, X.; Xia, Q.; Li, Z. Adsorption of CO_2 on Zeolite 13X and Activated Carbon with Higher Surface Area. *Sep. Sci. Technol.* **2010**, *45* (5), 710−719.

https://doi.org/10.1021/acs.energyfuels.4c03080
Energy Fuels 2024, 38, 22916−22925